# Criteria for recognition of localization and timing of multiple events of hydrothermal alteration in sandstones illustrated by petrographic, fluid inclusion, and isotopic analysis of the Tera Group, Northern Spain

**Laura González-Acebrón · R. H. Goldstein · Ramón Mas · José Arribas**

**Abstract** Stratigraphic relations, detailed petrography, microthermometry of fluid inclusions, and fine-scale isotopic analysis of diagenetic phases indicate a complex thermal history in Tithonian fluvial sandstones and lacustrine limestones of the Tera Group (North Spain). Two different thermal events have been recognized and characterized, which are likely associated with hydrothermal events that affected the Cameros Basin during the mid-Cretaceous and the Eocene. Multiple stages of quartz cementation were identified using scanning electron microscope cathodoluminescence on sandstones and fracture fills. Primary fluid inclusions reveal homogenization temperatures (Th) from 195 to 350°C in the quartz cements of extensional fracture fillings. The high variability of Th data in each particular fluid inclusion assemblage is related to natural reequilibration of the fluid inclusions, probably due to Cretaceous hydrothermal metamorphism. Some secondary fluid inclusion assemblages show very consistent data (Th = 281–305°C) and are considered not to have reequilibrated. They are likely related to an Eocene hydrothermal event or to a retrograde stage of the Cretaceous hydrothermalism. This approach shows how multiple thermal events can be discriminated. A very steep thermal gradient of 97–214°C/km can be deduced from $\delta^{18}O$ values of ferroan calcites ($\delta^{18}O$ −14.2/−11.8‰ V-PDB) that postdate quartz cements in fracture fillings. Furthermore, illite crystallinity data (anchizone–epizone boundary) are out of equilibrium with high fluid inclusion Th. These observations are consistent with heat-flux related to short-lived events of hydrothermal alteration focused by permeability contrasts, rather than to regional heat-flux associated with dynamo-thermal metamorphism. These results illustrate how thermal data from fracture systems can yield thermal histories markedly different from host-rock values, a finding indicative of hydrothermal fluid flow.

**Keywords** Quartz cements · Fluid inclusions · Thermal evolution · SEM-CL · Cameros basin

L. González-Acebrón (✉) · R. Mas
Dpto. Estratigrafía, Facultad de Ciencias Geológicas (UCM), Instituto de Geología Económica (CSIC), C/ Jose Antonio Novais 2, 28040 Madrid, Spain
e-mail: lgcebron@geo.ucm.es

R. H. Goldstein
Department of Geology, University of Kansas, 1475 Jayhawk Blvd., Lawrence, KS 66045, USA

J. Arribas
Dpto. Petrología y Geoquímica, Facultad de Ciencias Geológicas (UCM), Instituto de Geología Económica (CSIC), C/ Jose Antonio Novais 2, 28040 Madrid, Spain

## Introduction

Without significant fluid flow, the spatial and temporal distribution of diagenetic and low-grade metamorphic alteration in siliciclastic sequences is thought to be predictable on the basis of burial depth history, thermal regime, and composition (eg. Bjørlykke 1998; Morad et al. 2000). Relatively few studies, however, have examined the influence of significant flow of hydrothermal fluids on sandstone diagenesis and low-grade metamorphism (e.g., Rossi et al. 2002; Ochoa et al. 2007). In these hydrothermal systems, sandstone alteration departs from the predicted diagenetic model because of transport of heat, solvent, and solute. Research on hydrothermal alteration of carbonate

strata, in contrast, has received significant attention in recent years, resulting in the focus of an entire issue of a scientific journal and many other publications (e.g. Davies and Smith 2006). Discriminating hydrothermal from other regimes of diagenetic alteration is a key component in much of the recent literature on this subject (e.g. Machel and Lonnee 2002; Esteban and Taberner 2003; Hiemstra and Goldstein 2005; Davies and Smith 2006; Goldstein in press).

This study contributes to bringing siliclastic diagenesis and low-grade metamorphic studies up-to-speed by providing an example of a hydrothermally affected siliciclastic sequence. In doing so, it develops approaches for identifying where hydrothermal alteration in siliciclastics has occurred, and elucidates novel techniques to document hydrothermal alteration, involving cathodoluminescence petrography, fluid inclusions, and other geothermometers.

Detecting, dating, and determining the origin of multiple thermal events in sandstones subjected to diagenesis and low-grade metamorphism are challenging, due to the scarcity of applicable geothermometers, geobarometers, dating techniques, and problems with resetting during alteration (De Caritat et al. 1993; Essene and Peacor 1995, 1997). This commonly results in the oversimplified interpretations of thermal history. Systems subjected to hydrothermal alteration are particularly difficult to work with, as they may have experienced multiple short-lived pulses of fluid flow, each driven by different geologic mechanisms (e.g. Coveney et al. 2000). In this study, the integration of scanning electron microscope cathodoluminescence (SEM-CL) with fluid inclusion microthermometry (e.g. Goldstein and Rossi 2002) and other published work on timing has proven useful in reconstructing timing and origin of multiple hydrothermal events. For this, we study host rock and fracture fillings of Upper Jurassic sandstone of the Cameros Basin in Spain. Although it is understood that many of the fluid inclusions in low-grade metamorphic systems suffer from reequilibration, making straightforward interpretation of data difficult (e.g. Turgarinov and Vernadsky 1970; Lacazette 1990; Goldstein and Reynolds 1994), in this study, most of the fluid inclusion assemblages show signs of having been only partially reequilibrated. Thus, they still prove useful in interpreting thermal history thanks to a detailed petrographic analysis including SEM-CL on quartz cements. This study provides a model for how multiple hydrothermal events can be discriminated in sandstones.

The Cameros Basin represents one of the Mesozoic Iberian Basins and the only one that shows metamorphism in the Iberian Range (e.g. Mas et al. 2002, 2003). More specifically, the metamorphism affected a large proportion of the deposits of the Eastern Cameros Basin (e.g. Casquet et al. 1992; Mantilla-Figueroa et al. 2002). The basin infill is composed of a thick sequence of continental sedimentary rocks, generated under an extensional regime characterized by high rates of subsidence, from the Tithonian to the Early Albian. This research is focussed on Tithonian strata of the Tera Group, a thick succession deposited in the eastern sector of the Cameros Basin during its first rifting stage (Figs. 1 and 2).

Early on dynamo-thermal metamorphism was considered to have occurred during the infilling of the Cameros Basin (Guiraud and Seguret 1985; Golberg et al. 1988). This model of burial metamorphism is still maintained by other authors (Casas-Sáinz, Simón-Gómez 1992; Mata et al. 2001; Del Río et al. 2009). These studies are based on an interpretation of the basin structure as a synclinal basin. In contrast, the thermal evolution of the eastern sector of the basin has been studied using radiometric dating (K-Ar), mineral assemblages, crystal chemical parameters of phyllosilicates, chlorite thermometry, and isotopic thermometry of sulfide deposits. These studies recognized a thermal event (Casquet et al. 1992; Alonso-Azcárate et al. 1995; Barrenechea et al. 1995, 2000; Mantilla-Figueroa et al. 1998; Alonso-Azcárate et al. 1999; Mas et al. 2003), which was characterized as low- to very low–grade hydrothermal metamorphism (Late Albian-Coniacian).

Our study is focused on fluid inclusion microthermometric data from quartz in extensional fracture fillings in the Tera Group, which are the likely focus zones for hydrothermal fluids (San Felices section, SAN), and quartz overgrowth cements in areas away from the these zones (El Espino section, ESP). The filled fractures are observable in the field (SAN) and have been interpreted to form during the extensional stage of basin formation (Guiraud and Seguret 1985; Mantilla-Figueroa 1999; Mata et al. 2001). The principal aims of this paper are as follows: (1) to compare the thermal histories of fracture fillings and host rocks in a basin affected by a low-grade metamorphism taking in consideration both diagenetic and hydrothermal processes, (2) to characterize the water–rock interaction in hydrothermal systems, and (3) to develop approaches to discriminate between different low-grade metamorphic processes in sedimentary basins.

## Geological and stratigraphic setting

### Basin formation

The Cameros Basin in the northern Iberian Range (Fig. 1) forms part of the Mesozoic Iberian Rift System (Mas et al. 1993; Guimerà et al. 1995; Salas et al. 2001; Mas et al. 2002). Intraplate rifting was a consequence of a generalized extensional regime, which separated Iberia from Europe.

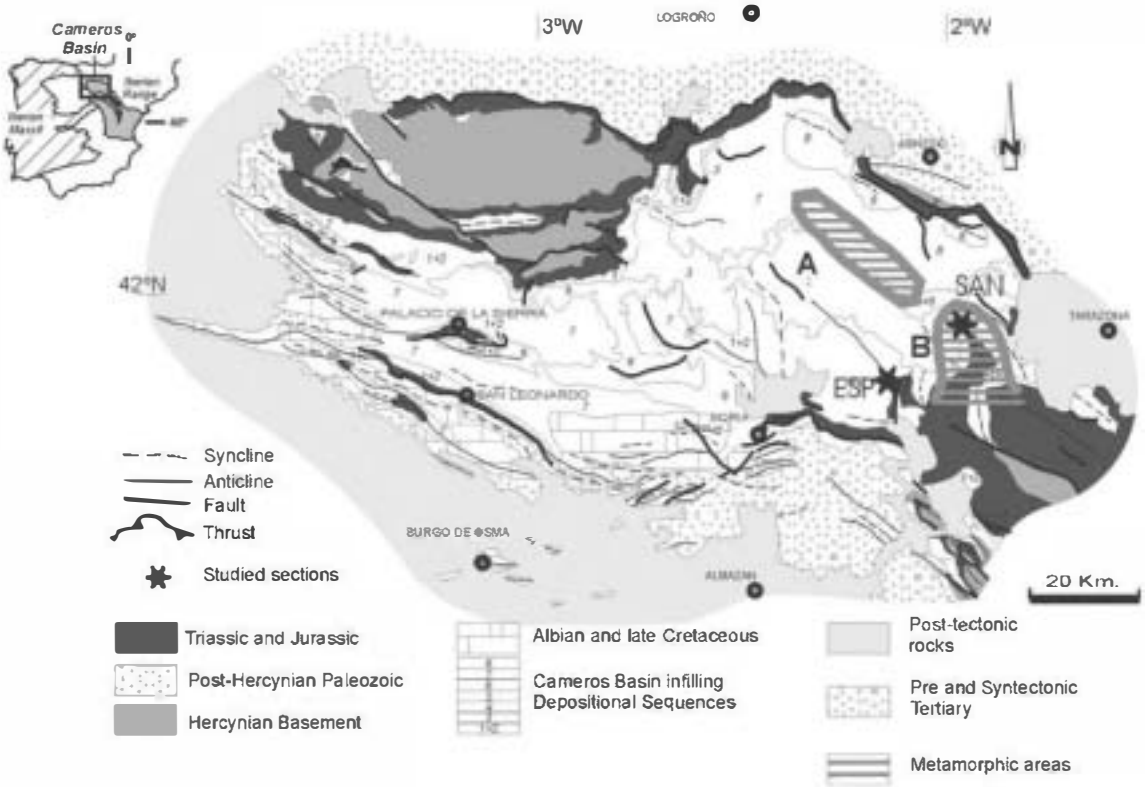


**Fig. 1** Geologic map of the Cameros Basin indicating the SAN section (El Pégado anticline) and the ESP section. The areas affected by low-grade and very low–grade hydrothermal metamorphism are indicated: **a** Yanguas-San Pedro Manrique area. **b** El Pégado anticline. Modified from Mas et al. (2002)

The subsidence and sedimentation rates in the Cameros Basin were very high, with vertical thicknesses up to 6 km and up to 9 km of stratigraphic record in the direction of the northward migration of depositional sequences recorded from the Tithonian to the early Albian. The basin has been interpreted as a hanging wall synclinal basin (extensional-ramp basin) formed over a roughly south-dipping ramp between two nearly horizontal sections (flats) in a deep extensional fault inside the Variscan Basement. The northern flat is 7 km depth and the southern flat 11 km depth (Guimerà et al. 1995). The direction of displacement for the hanging wall was S-SW, parallel to the direction of the basin extension (Mas et al. 1993, 2002, 2003; Guimerà et al. 1995, 2004). Alternatively, Guiraud and Seguret (1985), Casas-Saínz and Gil-Imaz (1998), Mata et al. (2001), Villalaín et al. (2003) and Casas-Saínz et al. (2009) interpreted the Cameros Basin as a synclinal basin, with vertical superposition of Lower Cretaceous sedimentary units rather than laterally juxtaposed bodies overlapping the prerift sequence. These authors consider a thrust fault to the north as a result of tectonic inversion of a normal fault generated at the beginning of the Cretaceous, which reached the Keuper facies in depth. This hypothesis has a mechanical flaw that makes it unlikely (Mas et al. 1993, 2002, 2003; Guimerà et al. 1995). The hypothesis of Guiraud and Seguret (1985) would require a slab of Jurassic rocks, only 500–800 m thick but more than 30 km wide and 100 km long, to be pulled from the South without suffering any break in continuity and without forming a fault over the ramp near the northern basin margin. This would have had to occur under subaerial conditions because of the continental nature of the rocks that filled the basin. Their model would require, an even more unlikely, later reverse displacement of tens of kms to the North, still somehow maintaining the continuity of the marine Jurassic substrate after the Cenozoic contraction.

## Basin infill

The basin record essentially consists of continental sedimentary rocks corresponding to alluvial and lacustrine systems, with rare marine incursions (Mas et al. 1993; Gómez-Fernández and Meléndez 1994). The sedimentary infill of the Cameros Basin has been divided into eight depositional sequences (Mas et al. 2002, 2003) (Fig. 2). The Tera Group represents the first stage of rifting sedimentation and is formed by two depositional sequences (DS 1 and DS 2, Fig. 2), which are Tithonian in age (Mas et al. 1993, 2004;

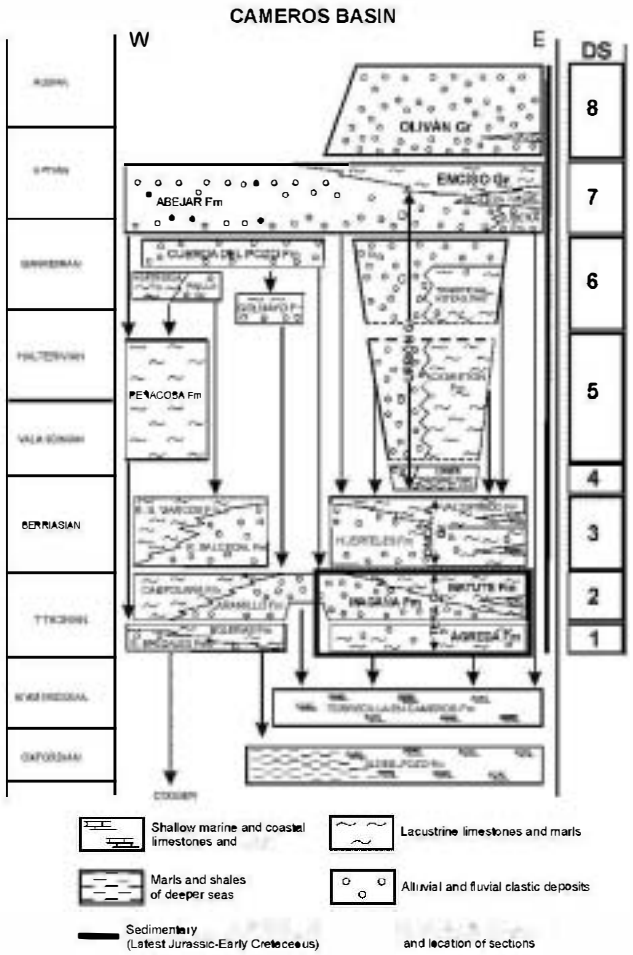


**Fig. 2** Stratigraphy of the depositional sequences (DS) of the Cameros Basin. The stratigraphic interval examined is indicated (Tera Group, DS 1 and DS 2). Modified from Mas et al. (2004)

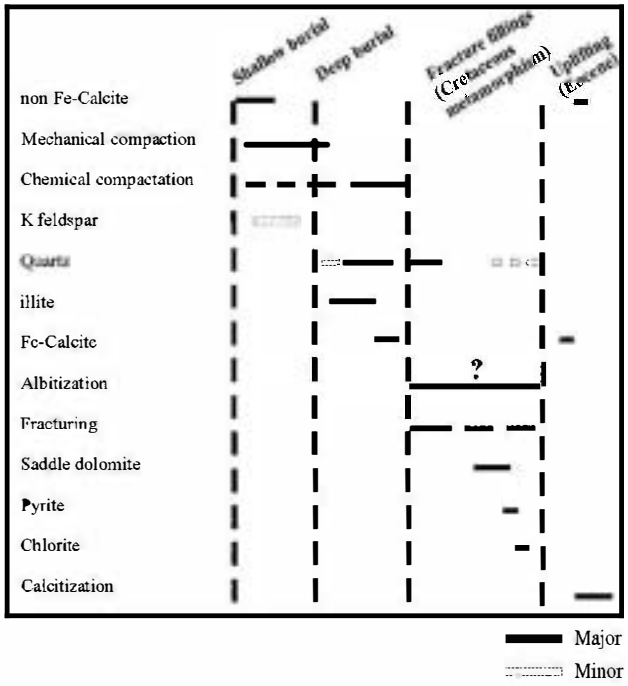


**Fig. 3** Sequence of processes and cements in sandstones of ESP and SAN sections. The kaolinite replacement over K-feldspars (epimatrix) has been totally replaced by illite. Muscovite and illite have been partially replaced by chlorite. Although the sequence is the same for both sections, the importance of the different diagenetic processes and products is not always the same. Mechanical compaction, calcitized saddle dolomite, pyrite, and chlorite are more abundant in SAN, whereas quartz overgrowth cement is more abundant in ESP

Martín-Closas and Alonso-Millán 1998). DS 1 is represented by siliciclastic fluvial fan facies and lacustrine–palustrine carbonate facies. The thickness of DS 1 is highly variable, with maximum thickness of 255 m. DS 2 is thick, up to 1,500 m in the depocenter, and consists of siliciclastic fluvial facies, which grade upwards and laterally to carbonate lacustrine facies. As in other rifted basins (Evans 1990; Garzanti et al. 2001, 2003), petrofacies indicate the erosion of prerift sedimentary substratum at the beginning of the rifting, followed by erosion of the basement in later stages (Arribas et al. 2003; González-Acebrón et al. 2007), defining a provenance cycle (Arribas et al. 2007). The sandstones in SAN section show a quartzofeldspathic framework composition (means: $Qm_{83}F_{15}Lt_2$ and $Qm_{85}K_9P_6$), with a dominance of plutonic rock fragments (Rg) over sedimentary (Rs) and metamorphic rock fragments (Rm) (mean: $Rg_{37}Rs_{35}Rm_{28}$, González-Acebrón et al. 2010). The porosity reduction of the sandstones occurred mainly by compaction (ICOMPACT = 0.90; Lundergard 1992). Mean framework sandstone composition of the ESP section is $Qm_{80}F_{16}Lt_4$ and $Qm_{84}K_7P_9$. Plutonic rock fragments (Rg) and sedimentary rock fragments (Rs) are predominant ($Rg_{45}Rs_{42}Rm_{13}$, González-Acebrón et al. 2010). The diagenetic sequence and ICOMPACT is similar to the SAN section (Figs. 3 and 4a), but there is greater development of quartz overgrowth in the ESP section (Fig. 4b).

## Metamorphic processes and studied sections

During the Late Albian to Coniacian, hydrothermal alteration affected the deposits of the eastern sector of the Cameros Basin (Casquet et al. 1992; Barrenechea et al. 1995; Alonso-Azcárate et al. 1995, 1999, 2002; Mantilla-Figueroa et al. 1998, 2002). The main features of this thermal alteration are as follows: (1) metamorphic grade is controlled by changes in rock composition and permeability rather than by burial depth (Alonso-Azcárate et al. 1995; Barrenechea et al. 1995, 2000, 2001); (2) thermal inversions across sections in the depocenter, for example in a single stratigraphic section Valanginian–Barremian deposits of the Urbion Group exhibit a higher metamorphic grade than the Tithonian and Berriasian deposits of Tera and Oncala older groups (Mantilla-Figueroa et al. 1998, 2002; Barrenechea et al. 2001); (3) postrift age of alteration

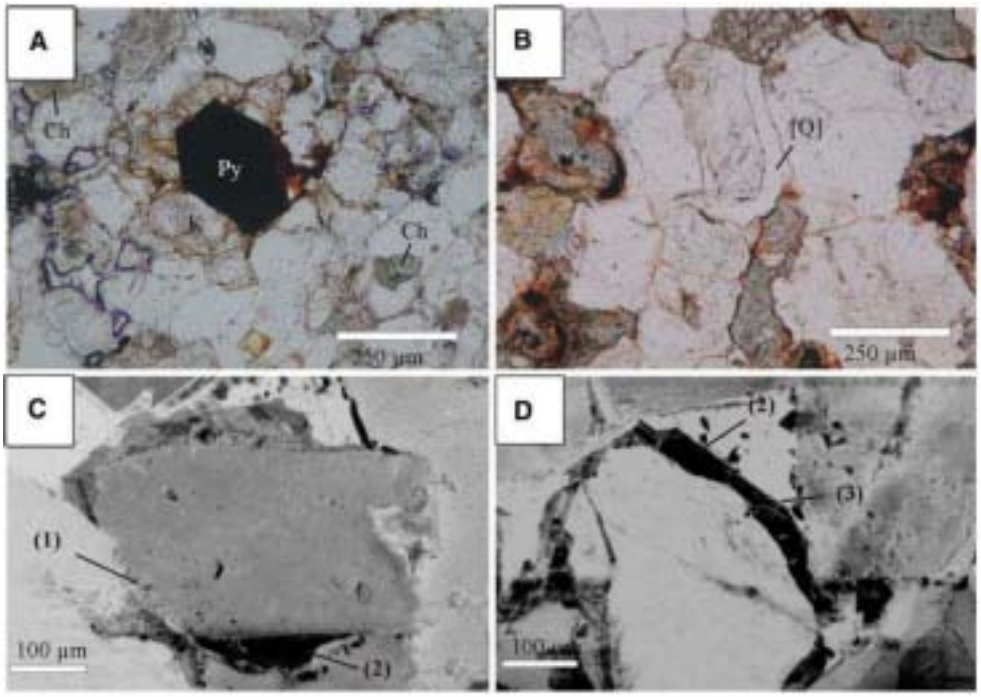


**Fig. 4** Petrography of ESP section. **a** Pyrite (Py) replacement of the sandstone framework. Notice the presence of K-feldspar (K) and chlorite (Ch). Plane-polarized light. **b** Quartz overgrowth ([Q]). Plane-polarized light. **c** Detrital quartz grain and two different quartz syntaxial overgrowths in SEM-CL. Overgrowth (1) is bright luminescent and shows relict fibrous texture. Overgrowth (2) is non-luminescent. **d** Detrital quartz grain and two different quartz cements in SEM-CL. Overgrowth (2) is non-luminescent and primary fluid inclusions have Th of 122–128°C. Overgrowth (3) shows banded luminescence and fills microfractures of the former overgrowth. First stages have Th of 127–128°C, followed by later fracture fillings with Th reaching 141°C. Numbers of the overgrowths correspond to the text and Table 5 of electronic supplementary material

(Late Albian to Coniacian, 107 ± 5 to 85 ± 6 Ma with K-Ar on authigenic illites), after the maximum burial stage, reached during the Early Albian (Casquet et al. 1992); and (4) metamorphic conditions from very low grade (anchizone) to low grade (epizone), with temperatures of 350–370°C at the metamorphic peak and maximum pressure of 1 kbar (Casquet et al. 1992; Barrenechea et al. 1995). Lines of evidence 1 and 2 point to a hydrothermal process rather than the regional metamorphic model suggested by Guiraud and Seguret (1985), Casas-Saínz and Gil-Imaz (1998), and Mata et al. (2001).

Figure 1 shows the location of the studied stratigraphic sections: SAN and ESP. The Tera Group was buried to 5,900 m from the Tithonian to Lower Paleogene at the first section (SAN). In the second section (ESP), the maximum burial depth for the same stratigraphic interval was probably 4,950 m (González-Acebrón 2009). Both burial depths are based on partial restored cross sections from Guimerà et al. (1995) and Mas et al. (2003).

The SAN section is located in the metamorphic area of El Pégado anticline (see B in Fig. 1). Illite crystallinity data in this section are between 0.23° and 0.30° $\Delta 2\theta$ (González-Acebrón 2009). Using the anchizone boundaries proposed by Kübler (1967, 0.42° and 0.25°), these values correspond to the anchizone–epizone boundary and are consistent with formerly published data of illite and chlorite crystallinity from the area (Mantilla-Figueroa 1999; Barrenechea et al. 2001). Mantilla-Figueroa et al. (2002) recognized a second very low–grade metamorphic process in this area as Eocene (45 ± 4 Ma) on the basis of radiometric dating (K/Ar) on authigenic illites (Mantilla-Figueroa 1999).

The ESP section is located outside of the zone of metamorphism (Fig. 1). The illite crystallinity data recorded in this section (0.47°-0.48° $\Delta 2\theta$, González-Acebrón 2009) are typical of diagenetic conditions.

## Methods

Samples were collected systematically from two representative stratigraphic sections of the Tera Group (SAN and ESP, Fig. 1), trying to represent the vertical variation of the host-rock sandstones (40 samples) and the variety of different minerals observed in the field in the fracture fillings (20 samples of fracture fillings; quartz, calcite, chlorite, and pyrite) to establish the paragenesis for host rock and for potential conduits for hydrothermal fluid flow. Doubly polished thick sections were prepared for the samples without

any heating and glued to frosted glass with cyanoacrilate. After optical petrographic analysis of the sections, selected areas of 5 of them were cut and removed from the glass using acetone. The microthermometric study was performed on these portions of samples in a Linkam THMSG-600 heating and freezing stage. The stage was calibrated with synthetic fluid inclusions, including triple point of $CO_2$, melting point of $H_2O$, and critical point of $H_2O$. Melting point of $H_2O$ standards shows that the accuracy for low-temperature measurements is better than ±0.1°C. Critical point standards show that accuracy for high-temperature measurements is better than ±1.0°C. Homogenization temperatures (Th) have been interpreted as minimum entrapment temperatures. In this case, no pressure corrections were applied because a pressure determination would involve too many error-prone assumptions without an independently obtained value of pressure. The interpretation of Th as minimum entrapment temperatures is a typical procedure in working with Th data (Goldstein and Reynolds 1994; Goldstein in press). To interpret salinity, a NaCl–$H_2O$ model was used on the basis of the observed first melting temperatures from fluid inclusions (Bodnar 1993).

Microthermometric and petrographic data were gathered on fluid inclusions in quartz and carbonate fracture fillings from SAN. From ESP, a microthermometric study on quartz overgrowths in sandstones was done. Due to the small size of the quartz overgrowths, this sort of study on quartz cements was not carried out in SAN sandstones. Four selected samples were mounted using aluminum stubs covered by carbon adhesive tape for SEM-CL. Subsequently, they were coated with carbon. Finally, they were studied under CL using a Gatan PanaCL photomultiplier-based CL detector installed on a Leo 1550 SEM. The operating conditions were 12-mm focal distance, 20-kV voltage, and 60-μm aperture.

A second group of 9 epoxy-mounted 100-μm-thick sections was prepared for stable isotope study on carbonate-bearing fracture fills from SAN. These sections were etched and stained using Alizarin Red S and potassium ferricyanide for carbonate identification (Lindholm and Finkelman 1972) after the CL study. Samples were taken using a microdrill and analyzed for $\delta^{13}C$ and $\delta^{18}O$. All sample powders were roasted *in vacuum* for one hour at 200°C to remove volatile organic contaminants and afterward reacted at 73°C in an automated carbonate reaction system (Kiel-III) coupled directly to the inlet of a Finnigan MAT 253 gas ratio mass spectrometer. Isotopic ratios were collected for $^{17}O$ contribution and are reported in per mil notation relative to the VPDB standard. Values were calibrated using NBS 19 as the primary standard. The precision of the analysis is 0.1‰ for both Oxygen and Carbon. Friedmann and O'Neil (1977) equation has been used for the calculations of $\delta^{18}O$ values from temperatures.

## Results

### Host-rock composition and diagenesis

The host rock of fracture fillings in the SAN section is composed of sandstone (subarkose and orthoquarzite) and lutite, with limestone and marl in the upper part. The diagenesis of the sandstone host rock includes different processes and cements, which have occluded the original porosity. This includes chemical compaction and stylolite formation (Fig. 3). SAN host rock contains pyrite crystals and chlorite nodules, producing a mottled texture and a greenish coloration. Related lacustrine and palustrine limestones are made up of mudstone to wackestone with ostracods and characea. Gypsum pseudomorphs in limestones occur near the top of the section. Lutites and marls are mainly composed of quartz, calcite, plagioclase, illite, and chlorite.

ESP section is composed of sandstones (subarkose) and minor conglomerates, with limestones and marl in the upper part. Limestones are also mudstones with ostracods and characea. In the sandstones, at least three different generations of syntaxial quartz overgrowth were identified with SEM-CL, showing primary fluid inclusion assemblages (FIAs) with first melting temperatures near −28°C. Clathrates have not been detected.

(1) *Bright luminescent overgrowth* is the earliest phase and precipitated with relict fibrous texture (1 in Fig. 4c). A primary FIA is identified on the basis of the distribution of the overgrowth, which is consistent with the distribution along the CL bands. The FIA has Th of 114–120°C and Tm ice between −10.6 and −10.3°C.

(2) *Non-luminescent syntaxial overgrowth* is the second growth phase and contains primary fluid inclusions with distribution consistent with the CL bands (2 in Fig. 4c and d). A consistent FIA shows Th of 122–128°C and Tm ice of −12.3/−11.6°C.

(3) *Banded luminescent quartz cement* fills microfractures in the earlier overgrowth (3 in Fig. 4d). First stages have primary fluid inclusions with Th that vary between 127 and 128°C, followed by later fracture fillings with Th that reach 141°C (Tm ice of −7.8°C) (Table 5 of electronic supplementary material).

### Fracture cements

Filled fractures appear in the SAN area and are typically subperpendicular to the stratification and 1 to 50 cm wide (Fig. 5a). They pinch out or reduce their width in incompetent layers, such as lutites and marls. Main minerals present in these fractures are quartz, ferroan and

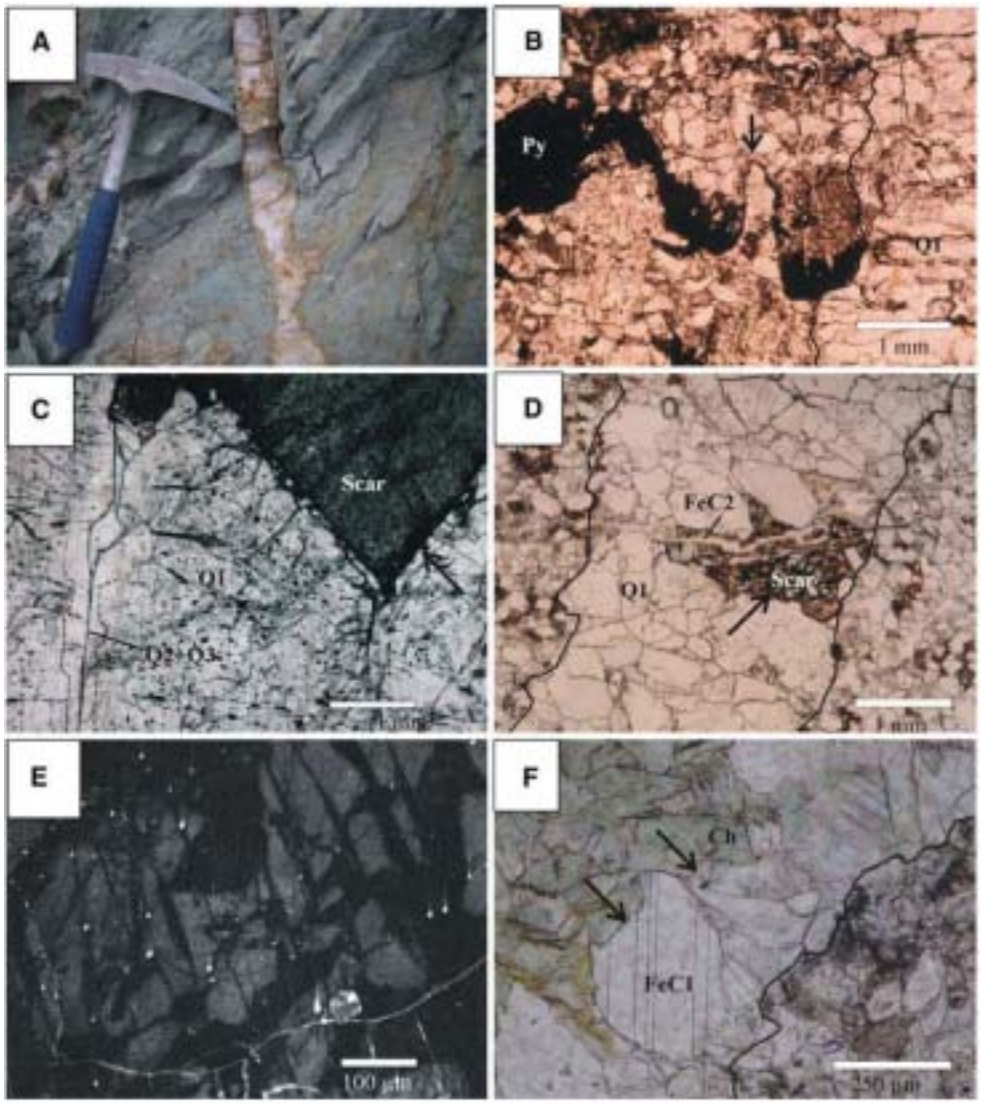


**Fig. 5** Petrography of the SAN section: **a** Field aspect of tensional fracture filling in the SAN section (El Pégado anticline). **b** Quartz vein (Q1) that postdates the stylolite (*arrow*). The vein is limited by a *line*. Py: pyrite. Plane-polarized light. **c** Two different quartz cements under plane-polarized light. The first one (Q1) corresponds to mottled quartz in SEM-CL (see picture E). The second one (Q2 + Q3) was precipitated after fracturing. Q2 and Q3 only can be distinguished under SEM-CL (Fig. 9). The *arrow* points to the corroded borders of quartz cement at the contact with the saddle carbonate (SCar). The sample was taken from the fracture of photo A (marked area in *dotted line* refers to Fig. 9). **d** Sandstone cut by a large fracture (between the *lines*), first filled with quartz (Q1) and later filled with saddle carbonate (SCar). This large fracture is also cut by a small fracture filled with ferroan calcite (FeC2). The *arrow points* to the corroded borders of quartz cement at the contact with the ferroan saddle carbonate. Plane-polarized light. **e** Mottled texture in quartz cement Q1 (SEM-CL) due to recrystallization associated with the metamorphic peak. A pattern of fracturing can be observed. The image represents an area in photo C. **f** Chlorite that postdates the ferroan calcite cement (FeC1). The corrosion is marked with *arrows*. Notice that both appear in a fracture that cut the sandstone framework (*right side of the line*), and the large size of the chlorite fans. Plane-polarized light

non-ferroan calcite, chlorite, and pyrite. Rarely, apatite crystals can be observed in thin section.

A common sequence of the fracture fillings was determined using conventional microscopy, CL, and SEM-CL petrography, together with the petrographic and microthermometric study of fluid inclusions (Fig. 6):

(1) *Quartz 1 (Q1)* cement postdates stylolites of the Tera Group sandstones (Fig. 5b). Q1 is homogeneous under transmitted light microscopy (see 1 in Fig. 5c and d) and shows a mottled texture in SEM-CL (Fig. 5e). Corrosion features are observed in Q1 where in contact with ferroan saddle dolomite cement (see arrows in Fig. 5c and d).

Q1 contains primary fluid inclusions of various sizes, with orientation and distribution related to growth. Measured fluid inclusions are between 1.5 and 5 µm with Th of

**Fig. 6** Sequence of processes and cements of the SAN tensional fracture fillings. Th of fluid inclusions, salinities (NaCl wt% NaCl eq.), $\delta^{18}$O and $\delta^{13}$C are shown on one axis. On the other hand, are the different processes, cements, and results listed in order, from older to younger

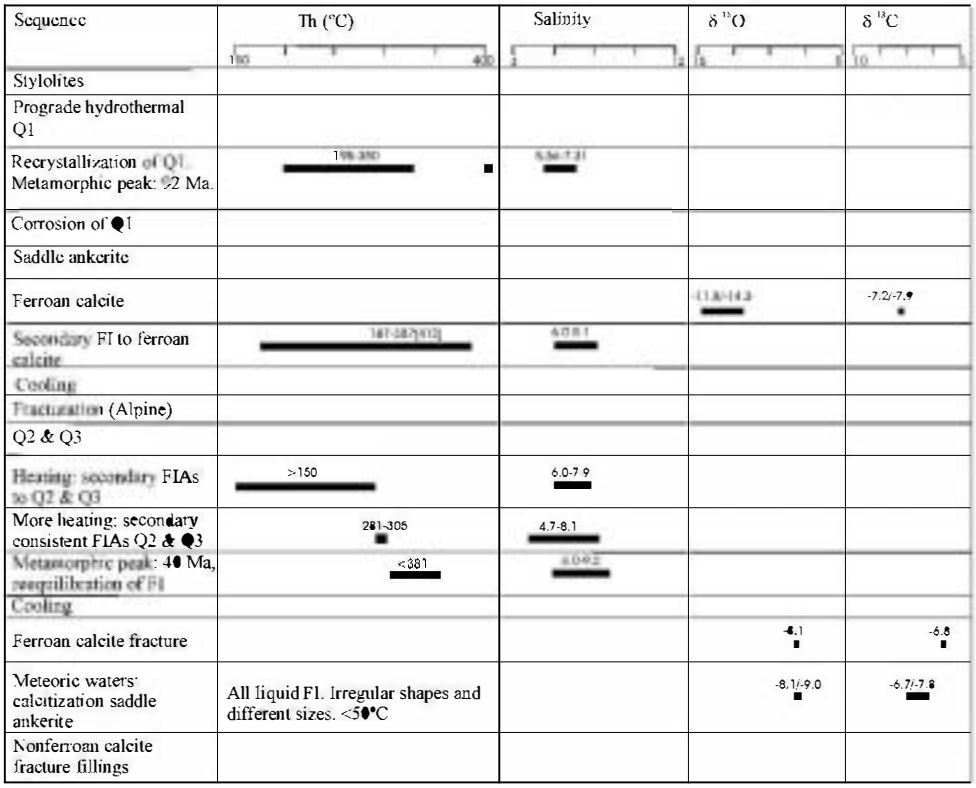


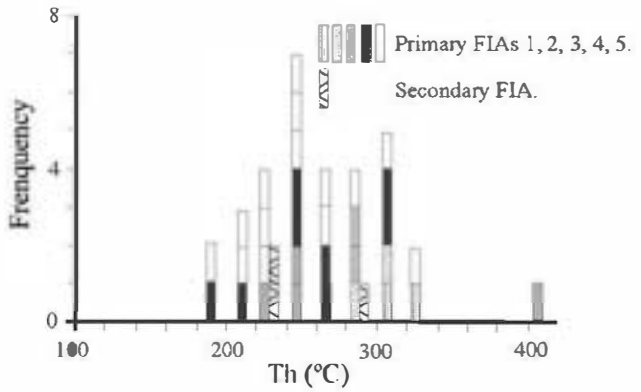


**Fig. 7** Frequency histogram of Th of primary fluid inclusions in Q1 cement (sample 4SAN-27) and some secondary FIA

194.8 and 350.2°C (Fig. 7 and Table 1 of electronic supplementary material) and Tm ice between −4.6 and −3.4°C. There is a single outlier with Th = 402.7–405.8°C. Th in FIAs are very inconsistent, as observed in Fig. 7. No petrographically paired vapor-rich and vapor-poor inclusions were observed, indicating that there is no evidence for necking down after a phase change (pinching off of single fluid inclusions to make multiple inclusions). No vapor-dominant inclusions were found, evidence against heterogeneous entrapment (e.g. Goldstein and Reynolds 1994). First melting temperatures (Te) are between −21 and −19°C. We observed that some fluid inclusions larger than 5 μm decrepitated on the stage during heating, usually at temperatures higher than 270°C. The presence of clathrates (gas hydrates) was detected. A vague freezing event other than the freezing of the aqueous phase was detected around −60°C. In some fluid inclusions, another freezing event was recorded around −180°C.

(2) *Saddle carbonate (SCar)* postdates Q1 (Fig. 5c and d) and exhibits a characteristic saddle habit with curved crystal faces and cleavage and sweeping extinction in cross-polarized light, as described by Radke and Matthis (1980) and Spötl and Pitman (1998). This non-ferroan calcite contains abundant solid inclusions or intergrowths of iron oxides and hydroxides, mainly concentrated along the cleavage planes.

Two different saddle carbonate phases can be distinguished. The earlier one (SCar1) is richer in iron oxide and hydroxide solid inclusions than the later one (SCar2), indicating two compositional zones: SCar1. Non-ferroan calcite, which is non-luminescent in CL, and SCar2. Non-ferroan calcite, which is bright luminescent in CL. In places, SCar1 totally have filled small voids and SCar2 only appears in the largest voids (>1 mm) where enough space was available for its precipitation. Both non-ferroan calcites contain abundant all-liquid fluid inclusions of variable sizes (2–16 μm). Stable isotopic compositions in both have very similar $\delta^{13}$C values between −7.8 and −6.6 (‰ V-PDB) and $\delta^{18}$O values between −9.0 and −8.1

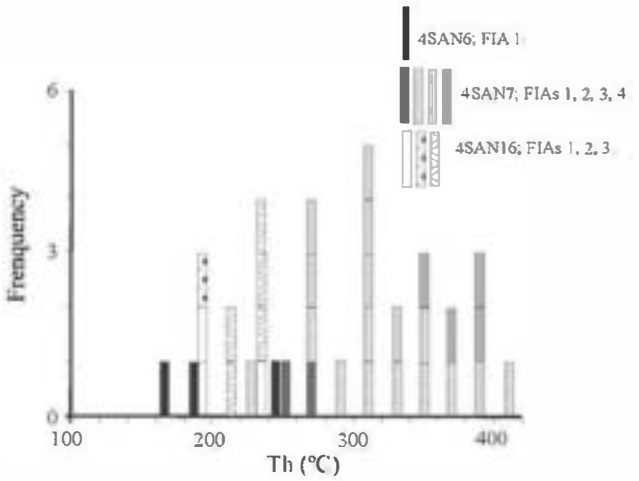


**Fig. 8** Frequency histogram of Th of secondary fluid inclusions in ferroan carbonate cements (samples 4SAN-6, 4SAN-7, 4SAN-16)

(‰ V-PDB) in non-luminescent calcite and $\delta^{13}C$ between −7.4 and −6.6 (‰ V-PDB) and $\delta^{18}O$ between −9.0 and −8.6 (‰ V-PDB) in the brightly luminescent calcite (Table 2 of electronic supplementary material).

(3) *Ferroan calcite (FeC1)* postdates the saddle carbonate (SCar). It normally shows dull luminescence in CL. It contains variably sized fluid inclusions (2.5–19 μm). Inclusions are typically secondary with Th = 168.0–412.7°C (Fig. 8) and Tm ice between −5.2 and −3.7°C (Table 3 of electronic supplementary material). Th values in FIAs are very inconsistent (Fig. 7).

Stable isotopes have values between −8.9 and −7.2 (‰ V-PDB) for $\delta^{13}C$ and between −14.3 and −11.8 (‰ V-PDB) for $\delta^{18}O$ (Table 2 of electronic supplementary material). The $\delta^{18}O$ values are progressively more negative with increasing depth in the section.

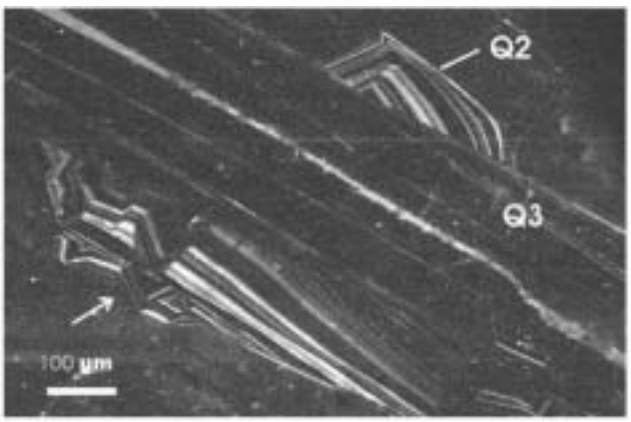


**Fig. 9** Two different quartz fracture fillings under SEM-CL. The photograph is taken in the fracture (Q1 + Q2) of Fig. 4c

(4) *Pyrite (Py)* crystals appear as part of the fracture fillings and also as replacement of the host rock. The pyrite typically has cubic shapes and variable sizes (from less than 1 mm to several centimeters). Quartz and chlorite encrust pyrite crystals where they replace the sandstone framework (Fig. 3). Based on this textural evidence, chlorite postdates pyrite in the fracture fillings.

(5) *Chlorite (Ch)* postdates and locally corrodes FeC1 (Fig. 5f). It displays green colors and coarse fan morphologies (100–200 μm). It has a magnesium-ferroan composition as has been determined by electron microprobe analysis.

(6) *Quartz 2 (Q2)* postdates at least Q1 and the saddle carbonate (SCar). Q2 fills small fractures that cut the mottled structure of Q1 (Fig. 9). Thus, a fracturing event is deduced between Q1 and Q2. Q2 bears primary growth fabrics displaying concentric growth zones of luminescent and non-luminescent quartz as well as some sector zoning (Fig. 9).

(7) *Quartz 3 (Q3)* cement cuts Q2 and is a non-luminescent fracture fill (Fig. 9). Under conventional petrography, Q2 and Q3 look like a single quartz cement phase (Fig. 5c). Q3 fills small fractures that postdate Q2 and can be distinguished in CL. Secondary fluid inclusions in Q2 and Q3 show Th of 281.2–305.2°C in some FIAs with consistent Th, with Tm ice between −5.2°C and −4.9 (Table 4 of electronic supplementary material and Fig. 10). FIAs with inconsistent Th are also present, showing Th lower and higher than the consistent ones. Two different groups can be distinguished: 1. FIAs with lower Th than the consistent FIAs (Th from 150 to

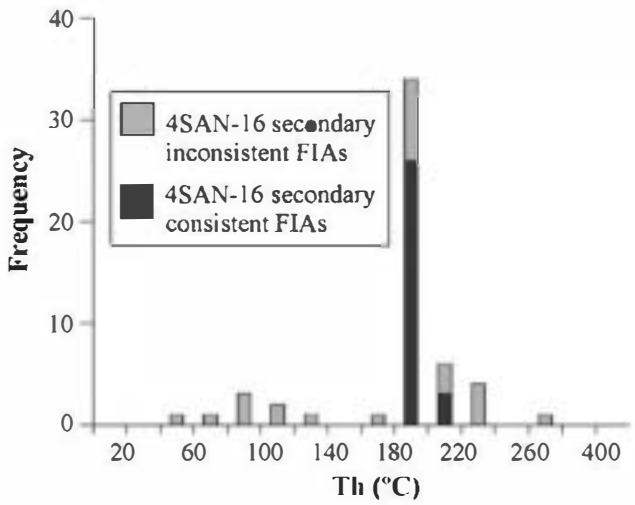


**Fig. 10** Frequency histogram of Th of secondary fluid inclusions in Q2 and Q3 cements. Notice the distinction between consistent and inconsistent FIAs. Sample 4-SAN-16

280°C) and 2. FIAs with higher temperature than the consistent FIAs (Th from 305 to 380°C). None of the inclusions in all FIAs show petrographic pairing or vapor-rich inclusions. Hence, no evidence of necking down after phase changes or heterogeneous entrapment was found.

(8) *Ferroan calcite (FeC2)* cement has filled small fractures (<2 mm) that cut all the former fracture fillings until chlorite formed. There is no textural evidence that FeC2 postdates Q2 and Q3. Stable isotope compositions of this cement are $\delta^{13}C = -6.8$ (‰ V-PDB) and $\delta^{18}O = -8.1$ (‰ V-PDB, Table 2 of electronic supplementary material).

(9) *Non-ferroan calcite (NFeC)* has filled the remaining space reduced by FeC2. Because of the small size of this cement (<1 mm), no isotopic analyses were performed.

## Discussion and interpretation

### Thermal events deduced from fracture fillings

#### *First metamorphic event*

Petrographic characteristics of cements, microthermometry data from fluid inclusions, and isotopic compositions permit the reconstruction of the sequence of thermal events during fracture filling of the Tera Group (SAN section):

*Quartz (Q1)* Deduced salinities of Q1 are between 5.6 and 7.3 wt% NaCl eq. Minor amounts of other ions are also likely. $CO_2$ and $CH_4$ are significant components deduced by the clathrate melting events and analyses using Raman microprobe on similar inclusions (Mantilla-Figueroa 1999).

There are several pieces of evidence to relate these primary fluid inclusions to a hydrothermal process:

(A) Th (194.8–350.6°C) are too high to be burial temperatures. Assuming a geothermal gradient of 30°C/km (Blackwell 1971; Waples 1980; Hitchon 1984), with a surface temperature of 20°C, estimated burial temperature at the maximum burial depth would have been no more than 180°C.

(B) The variability of Th data in each particular fluid inclusion assemblage (Table 1 of electronic supplementary material and Fig. 7) probably is due to natural thermal reequilibration of the fluid inclusions. Outlier values may indicate the most extreme examples of thermal reequilibration. Stretching and decrepitation are typical processes of fluid inclusions in metamorphic systems (Goldstein and Reynolds 1994). Alternatively, necking down after a phase change can lead to a few high values, but there is no petrographic evidence supporting this.

(C) The mottled texture of quartz (Q1) in SEM-CL (Fig. 5e) is interpreted as a recrystallization fabric. The development of this mottled fabric is consistent with the metamorphism interpreted by Casquet et al. (1992) as Cretaceous in age. Recrystallization features of quartz overgrowths previously have been described by Goldstein and Rossi (2002) in sandstones and in hydrothermal veins (e.g., Rush and Reed 2005; Rush et al. 2006).

*Saddle carbonate (SCar)*: The non-ferroan calcite composition of SCar is very likely a replacement of saddle dolomite or ankerite, because these are the typical minerals that form saddle carbonate (Radke and Matthis 1980 and Spötl and Pitman 1998). The all-liquid primary fluid inclusions support recrystallization at low temperature. Similar ankerite cement has been identified by Benito et al. (2001, 2006) in the underlying Kimmeridgian limestones, and these authors associated this cement with the Cretaceous hydrothermal metamorphism of the basin followed by low-temperature recrystallization.

*Ferroan calcite (FeC1)*: The deduced salinities in the secondary fluid inclusions of FeC1 are between 6.01 and 8.14 wt% NaCl eq. (Fig. 8 and Table 3 of electronic supplementary material). The Th data of secondary fluid inclusions of FeC1 in the same range as the primary fluid inclusions described for quartz (Q1), as well as the high variable Th data, point to reequilibration of these secondary fluid inclusions during the Cretaceous metamorphism. In the absence of primary fluid inclusions, stable isotope data are useful in estimating the origin of FeC1. The very negative $\delta^{18}O$ values are best explained by precipitation at high temperature (around 200–400°C), as the FeC1 postdates Q1 and predates chlorite. In addition, the negative values of $\delta^{13}C$ can be interpreted as being inherited from a system in which waters were derived from an overlaying source probably related with subaerial exposure that favoured a localized input of highly $^{13}C$-depleted soil–gas $CO_2$ (Benito et al. 2001, 2006).

*Pyrite and chlorite*: Both the literature and the former established paragenesis suggest that Q1, SCar, FeC1, pyrite, and chlorite are metamorphic phases related to the Cretaceous hydrothermal event (Alonso-Azcárate et al. 1999; Mata et al. 2001; Benito et al. 2001, 2006). The large size of the fan morphologies of chlorite is also evidence of high-temperature growth (Fig. 5f). Thus, primary fluid inclusions of Q1 must be related to this Cretaceous thermal alteration. On the basis of CL petrography, the inclusions appear to have been trapped during recrystallization of the Q1 cement. This could indicate that the Cretaceous hydrothermal alteration could have reached temperatures

of at least 350–410°C (maximum Th of primary fluid inclusions to Q1 and of secondary fluid inclusions to FeC1).

A post-Cretaceous, second thermal event is interpreted on the basis of radiometric dating (Mantilla-Figueroa et al. 2002) and has been related to the inversion of the basin during the Eocene (Alpine Orogeny). Thus, we have to consider the alternative hypothesis that primary fluid inclusions of Q1 reequilibrated during Eocene heating. In this case, the inclusions would reflect the conditions of the second thermal event. This hypothesis could be supported by similar salinities between fluid inclusions primary to Q1 (5.56–7.31 wt% NaCl eq.) and fluid inclusions secondary to Q2 and Q3 (4.73–8.14 wt% NaCl eq.).

A Cretaceous age is more likely, however, because no consistent FIAs were found in Q1 which exhibits recrystallized textures. These observations suggest that a thermal maximum may have been reached during the Cretaceous hydrothermalism and that this thermal process was responsible for the reequilibration of primary inclusions and recrystallization in Q1.

## The steep thermal gradient as a consequence of hydrothermal processes

The similar petrographic character, paragenesis, and chemical composition of FeC1 in all fracture fillings allow us to assume same or similar age and fluid composition for FeC1 throughout the studied section. Given the same fluid isotopic composition precipitating FeC1 throughout the section, the upward increase in $\delta^{18}O$ indicates a steep paleogeothermal gradient. The maximum difference in vertical stratigraphic position between analyzed samples is 370 m. The paleotemperatures have been calculated for two possible scenarios: (1) in which the sediment with the deepest burial precipitated at 200°C and (2) a deep burial precipitation temperature of 300°C. These temperatures were chosen because 200°C is close to the lowest temperature of primary fluid inclusions of Q1 (194.8°C) and 300°C is close to the highest temperature of these fluid inclusions (350.6°C). Given the first scenario (200°C), the data indicate a metamorphic gradient of 153°C/km in the lower part and 72°C/km in the upper part of the section (Fig. 11). Given the second scenario (300°C), the data indicate a gradient of 276°C/km in the lower part and 121°C/km in the upper part of the section (Fig. 11). This steep and decreasing gradient from the bottom to the top is probably due to a rapid injection of hot fluids into cooler rocks, associated with hydrothermal processes. The calculated values of $\delta^{18}O$ of the water are between 6.5 and 13.0 (‰ V-SMOW) for the proposed temperatures (300 and 200°C, respectively). These are typical values of metamorphic waters (Taylor 1974). A similarly high geothermal gradient is recorded for the Cobre-Babilonia hydrothermal vein system (170–200°C/km) by Camprubí et al. (2006).

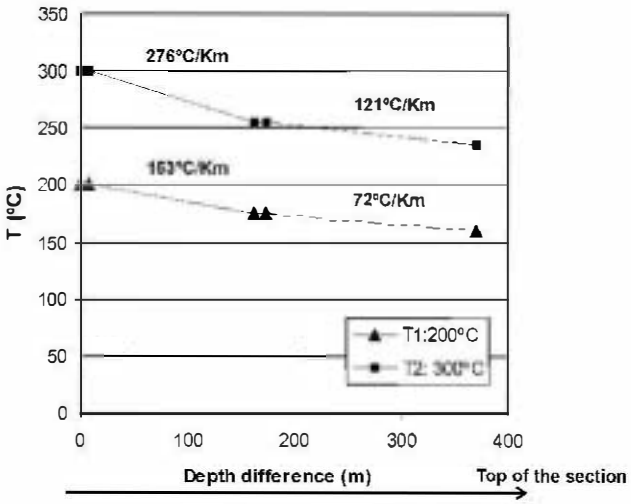


**Fig. 11** Paleogeothermal gradient recorded using $\delta^{18}O$ values of the FeC1 in 5 samples of different burial depth of the SAN section. The *x* axis indicates the depth difference among samples. Notice the decrease in the gradient to the top of the section

*Second metamorphic event*

*Quartz (Q2 and Q3)*: Consistent Th values (Th = 281.2–305.2°C) in secondary FIAs in Q2 and Q3 can be related either to (1) a retrograde stage of Cretaceous hydrothermalism or to (2) a later event of thermal alteration. We consider the second possibility more likely for the following reasons: (1) the saddle dolomite or ankerite precipitated between the mottled quartz cement (Q1) and the two different quartz stages (Q2 and Q3) that fill the later fractures; (2) FIAs are not reequilibrated; thus, they probably have not experienced much overheating after their entrapment; (3) the FIAs postdate the recrystallization of quartz, which may have been associated with the Cretaceous metamorphism.

Q2 and Q3 may postdate the Cretaceous metamorphism because quartz has not recrystallized. The lower Th of the consistent FIAs in Q2 and Q3 compared to Q1 Th indicate that the thermal peak was reached before entrapment of the FIAs in Q2 and Q3. High temperatures in these secondary inclusions, higher than would normally be ascribed to burial, could be indicative of their entrapment during the late (cooling) stages of Cretaceous hydrothermalism or during Eocene hydrothermalism. Deduced temperatures using chlorite microthermometry for the Eocene alteration (Mantilla-Figueroa et al. 2002) are in the same range (290°C) as fluid inclusion Th (281.2–305.2°C). Thus, we consider the Eocene hypothesis more probable. Lower Th FIAs (150–280°C) were probably trapped earlier and the

higher Th FIAs (305–380°C) trapped later. The increasing temperatures would cause thermal reequilibration of lower temperature fluid inclusions.

*Later processes*

*Ferroan and non-ferroan calcite (FeC2 and NFeC)*: Last fracture fillings are probably related to the alpine contraction influx of meteoric waters. Meteoric waters are also responsible for the calcitization of the saddle dolomite or ankerite. Evidence of recrystallization due to meteoric water is:

(1) All-liquid fluid inclusions entrapped during recrystallization indicate that the calcitization process probably was below about 50°C following Goldstein and Reynolds' (1994) criteria.
(2) Non-ferroan composition of NFeC and the presence of solid inclusions of ferroan oxides and hydroxides in the NFeC are related to the original phase of precipitation (saddle dolomite or ankerite).
(3) The negative $\delta^{18}O$ values for SCar1 and SCar2, due to replacement by non-ferroan calcite, are similar to what would be expected for calcite precipitation from a low-temperature fluid with $\delta^{18}O$ of the present-day groundwater (−9.5 to −9.1‰, V-SMOW, Plata 1994) with median temperatures of 13°C (Spanish Geological Survey, unpublished data). Calcite precipitating under these conditions would have a $\delta^{18}O$ of −9.4 to −9.8‰.
(4) The relatively invariant values for the $\delta^{18}O$ and the negative values for the $\delta^{13}C$ are typical of meteoric diagenesis (Allan and Mattews 1982; James and Choquette 1990).

The very similar isotopic values for SCar1 and SCar2 (Table 2 of electronic supplementary material) indicate that they were probably recrystallized by a similar low-temperature meteoric fluid. Figure 12 resumes the diagenetic and metamorphic evolution of a hypothetical sandstone sample of the Tera Group in SAN section in relation to the basin development.

Difference between fracture fills and host rock

Evidence for a lack of equilibrium between the host rock and the high temperatures in fracture fillings is important in constraining the thermal alteration as hydrothermal. The lack of equilibrium indicates that hot fluids were focused along fractures. Minimum fluid inclusion–based temperatures in fractures reached 400°C, whereas the X-ray diffraction data from lutites in the host rock point to lower temperatures (anchizone–epizone boundary: Mantilla-Figueroa 1999; Barrenechea et al. 2001). This difference is probably related to the low permeability of the host rock at the moment of the Cretaceous hydrothermal alteration, and focus of fluids along fractures, leading to different thermal histories in host rock versus fractures, or short-lived fluid flow that did not allow equilibration of the host rock.

Quartz diagenesis in the host rock

The ESP section preserves a record of sandstone diagenesis in an area lacking evidence for major hydrothermal alteration. Clathrates have not been detected, indicating lower gas contents than fluid inclusions measured from the SAN area. Fluid inclusions in the syntaxial quartz overgrowths indicate precipitation during progressive burial from high-salinity fluids generating the following sequence:

(1) *Bright luminescent quartz overgrowth* (see number 1 in Fig. 4c) interpreted as a pseudomorphic replacement of chalcedony or some less stable silica precursor based on its relict fibrous texture (e.g. Goldstein and Rossi 2002). Assuming a geothermal gradient of 30°C/km, Th of this cement implies the burial depths of at least 3,100–3,300 m, consistent with a late Barremian-early Aptian age or later, based on the reconstructions of Mas et al. (2002, 2003). Salinities from Tm ice measurements are between 14.3 and 14.6 wt% NaCl eq. (Table 5 of electronic supplementary material).
(2) *Non-luminescent quartz overgrowth* (see number 2 in Fig. 4c and d, Table 5 of electronic supplementary material) suggests by its Th a burial depth of at least 3,400–3,600 m, consistent with a late Aptian–early Albian age or later, based on the reconstructions of Mas et al. (2002, 2003). Thus, syntaxial quartz overgrowths (1) and (2) are most easily interpreted as predating Cretaceous thermal alteration (late Albian–Coniacian). Salinities from Tm ice measurements of phase 2 FIAs are between 15.8 and 16.2 wt% NaCl eq.
(3) *Banded luminescent quartz cement* (see number 3 in Fig. 4d) is probably related to a deeper burial than the FIAs of stage 2, because it postdates quartz cement phases (1) and (2) and has higher Th. Salinities from Tm ice measurements are between 11.5 and 12.1 wt% NaCl eq.

Temperature data from ESP syntaxial cements probably predate temperature data from fracture fillings at SAN, because fracture fillings cut quartz syntaxial overgrowths. The influence of major hydrothermal processes has not been recorded at ESP, as pointed out by the illite crystallinity (diagenetic field, González-Acebrón 2009) and fluid inclusion microthermometry. As far as the lithologies and age of the host rocks are equivalent in both sections, this

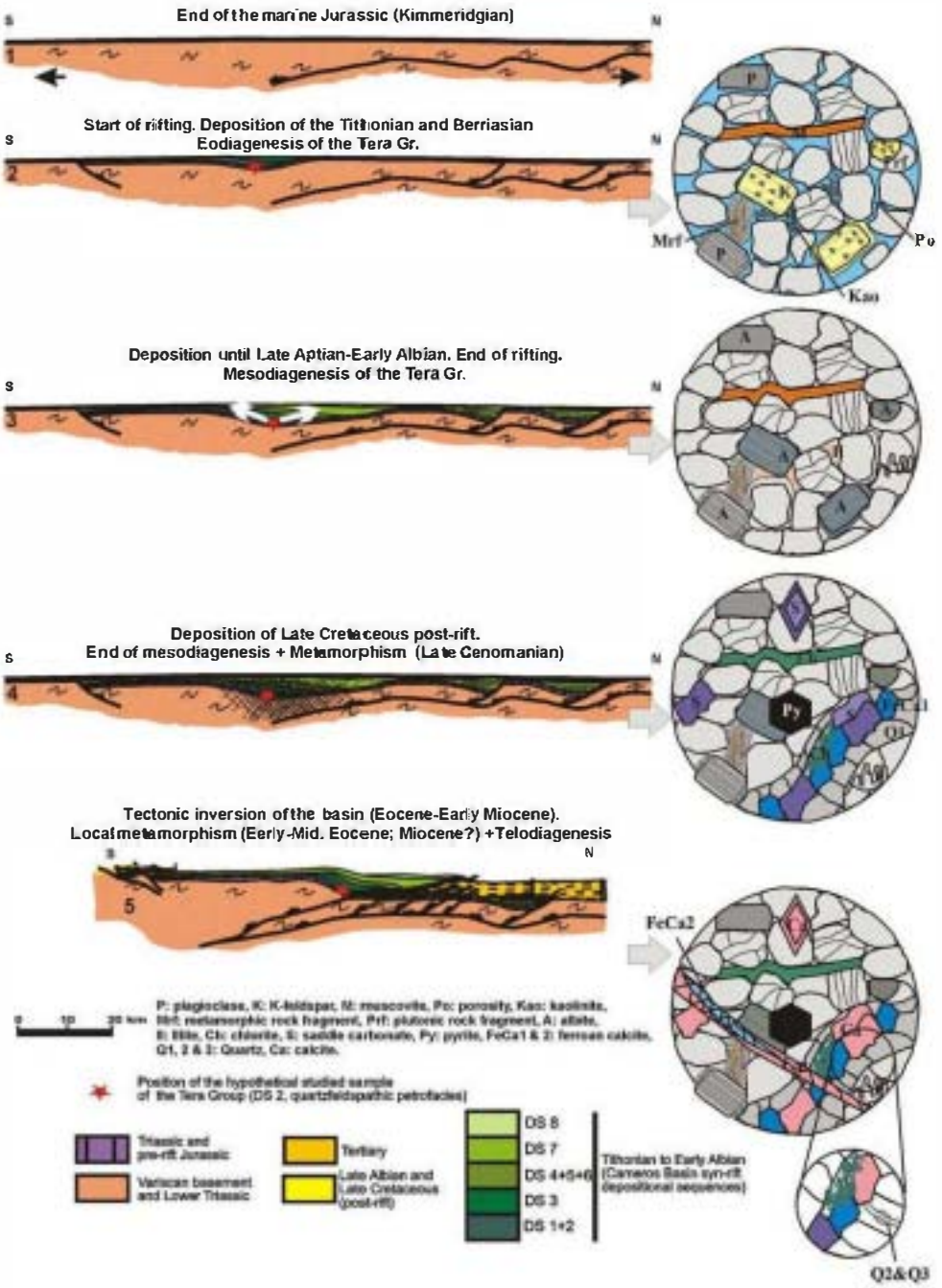


**Fig. 12** Geological sketch for the diagenetic and metamorphic evolution of a hypothetical sandstone sample of the Tera Group in SAN (Magaña Fm., DS 2)

work confirms the local nature of hydrothermal alteration as independent of the burial history.

## Conclusions

(1) The effects of different metamorphic events can been recognized in the same fracture fillings, based on detailed petrography, stable isotopes, and microthermometry of fluid inclusions. Fluid inclusions combined with SEM-CL are the essential tool, in this case, to help delineate the thermal history of very low–grade to low-grade metamorphism from hydrothermal alteration. The fact that fluid inclusion assemblages typically partially reequilibrate during metamorphism aids in the determination of thermal history.

(2) Evidence of quartz recrystallization has been found using SEM-CL in syntaxial overgrowths and fracture fillings, related to very low–grade to low-grade

metamorphism. They include fibrous textures from a less stable silica precursor, mottled texture, and reequilibrated Th from fluid inclusions. At least three different quartz fracture fillings separated by two fracturing events have been recognized in the same fracture using SEM-CL. Despite recrystallization and multiple events of quartz precipitation, aspects of thermal history in these metamorphic systems can be discriminated.

(3) Stable isotopic data are used to show that a steep geothermal gradient of 153–276°C/km in the lower stratigraphic intervals decreased upward to 72–121°C/km in the upper stratigraphic intervals. Such abnormal gradients are one hallmark of hydrothermal fluid flow, and changes in gradient can help to delineate pathways of fluid flow.

(4) One Cretaceous as well as one Eocene event of hydrothermal alteration can be discriminated on the basis of radiometric dating, petrographic relationships, and fluid inclusion data. This approach for discriminating between different thermal events has widespread applicability in systems where timing and origin of multiple thermal events are normally not routinely discriminated. Our research should encourage other researchers that this discrimination is possible.

(5) High paleotemperatures in fracture fillings in the Tera Group are out of equilibrium with host rock (illite crystallinity data). These differences are probably due to the low permeability of the host-rock and short-term hydrothermal fluid flow through fractures. This lack of equilibrium between fracture-fill paleotemperatures and host-rock paleotemperatures is strong evidence of hydrothermal alteration and preferential focus of fluids through fractures. Similar comparisons can be made elsewhere, in other metamorphic systems, to discriminate between hydrothermal and other forms of heating.

**Acknowledgments** Funding for this research was provided by the Spanish DIGICYT projects BTE 2001-026, CGL 2005-07445-C03-02/BTE and CGL2008-01648/BTE, and by UCM-CM (Universidad Complutense-Madrid Community) for the Research Group "Sedimentary Basin Analysis" for the present contract of the first author. The authors would like to thank Barrenechea, J.F. and Rankey, E. for their useful suggestions and Shinonge, H., Cane, G., Herrero, G., Moral, B., and Barajas, M.A. for their technical support. This manuscript benefits by the useful comments of C. Augustsson and an anonymous referee.

## References

Allan AR, Mattews RK (1982) Isotope signatures associated with early meteoric diagenesis. Sedimentology 29:797–817

Alonso-Azcárate J, Barrenechea JF, Rodas M, Mas R (1995) Comparative study of the transition between very low-grade metamorphism and low-grade metamorphism in siliciclastic and carbonate sediments. Early Cretaceous, Cameros Basin (North Spain). Clay Miner 30:407–419

Alonso-Azcárate J, Rodas M, Bottrell SH, Raiswell R, Velasco F, Mas R (1999) Pathways and distances of fluid flow during low-grade metamorphism: evidence from pyrite deposits of the Cameros Basin, Spain. J Metamor Geol 17(4):339–348

Alonso-Azcárate J, Rodas M, Bottrell SH, Mas R (2002) Los yacimientos de pirita de la Cuenca de Cameros, Zubía. Instituto de Estudios Riojanos 14:173–190

Arribas J, Alonso A, Mas R, Tortosa A, Rodas M, Barrenechea JF, Alonso-Azcarate J, Artigas R (2003) Sandstone petrography of continental depositional sequences of an intraplate rift basin: Western Cameros Basin (North Spain). J Sediment Res 73(2):309–327

Arribas J, Ochoa M, Mas R, Arribas ME, González-Acebrón L (2007) Sandstone petrofacies in the northwestern sector of the Iberian Basin. J Iberian Geol 33(2):191–206

Barrenechea FJ, Rodas M, Mas JR (1995) Clay mineral variation associated to diagenesis and low-grade metamorphism of early Cretaceous sediments in the Cameros Basin, Spain. Clay Miner 30:89–103

Barrenechea FJ, Rodas M, Frey M, Alonso-Azcárate J, Mas JR (2000) Chlorite, Corrensite and Chlorite- Mica in Late Jurassic Fluvio-Lacustrine sediments of the Cameros Basin of Northeastern Spain. Clay Clay Miner 48(2):256–265

Barrenechea FJ, Rodas M, Frey M, Alonso-Azcárate J, Mas JR (2001) Clay diagenesis and low-grade metamorphism of Tithonian and Berriasian sediments in the Cameros Basin. Clay Miner 36(3):325–333

Benito MI, Lohmann KC, Mas R (2001) Discrimination of multiple episodes of meteoric diagenesis in a Kimmeridgian reefal complex, north Iberian Range, Spain. J Sediment Res 71(3):380–393

Benito MI, Lohmann KC, Mas R (2006) Micro-sized dolomite inclusions in ferroan calcite cements developed during burial diagenesis of Kimmeridgian reefs, Northern Iberian Basin, Spain. J Sediment Res 76:472–482

Bjørlykke K (1998) Clay mineral diagenesis in sedimentary basins—a key to the prediction of rock properties. Examples from the North Sea Basin. Clay Miner 33:15–34

Blackwell DD (1971) The thermal structure of the continental crust. In: Heacock JG (ed) The structure and physical properties of the earth's crust. Geophysical Monograph 14, pp 169–184

Bodnar RJ (1993) Revised equation and Table for determining the freezing point depression of H2O-NaCl solutions. Geochim Cosmochim Acta 57:683–684

Camprubí A, González-Partida E, Torres-Tafolla E (2006) Fluid inclusions and sTable isotope study of the Cobre-Babilonia polymetallic epithermal vein system, Taxco district, Guerrero, Mexico. J Geochem Exp 89:33–38

Casas-Sáinz AM, Simón-Gómez JL (1992) Stress field and thrust kinematics: a model for the tectonic inversion of the Eastern Cameros Basin, Northern Spain. Geol Rudsch 86:802–818

Casas-Saínz AM, Gil-Imaz A (1998) Extensional subsidence, contractional folding and thrust inversion of the Eastern Cameros Basin, Northern Spain. Geol Rudsch 86:802–818

Casas-Saínz AM, Villalaín JJ, Soto R, Gil-Imaz A, Del Río P, Fernández G (2009) Multidisciplinary approach to an extensional syncline model for the Mesozoic Cameros Basin (N Spain). Tectonophys 470:3–20

Casquet C, Galindo C, González-Casado JM, Alonso A, Mas R, Rodas M, García E, Barrenechea JF (1992) El metamorfismo en la Cuenca de Los Cameros. Geocronología e implicaciones tectónicas. Geogaceta 11:22–25

Coveney RM Jr, Ragan VM, Brannon JC (2000) Temporal benchmarks for modeling Phanerozoic flow of basinal brines and hydrocarbons in the southern midcontinent based on radiometrically dated calcite. Geol 28:795–798

Davies GR, Smith T (2006) Structurally controlled hydrothermal dolomite reservoir facies: an overview. AAPG Bull 90:1641–1690

De Caritat P, Hutcheon I, Walshe J (1993) Chlorite geothermometry: a review. Clay Clay Miner 41:219–239

Del Río P, Barbero L, Mata P, Fanning CM (2009) Timing of diagenesis and very low-grade metamorphism in the eastern sector of the Sierra de Cameros (Iberian Range, Spain): a U-Pb SHRIMP study on monazite. Terra Nova 21:438–444

Essene EJ, Peacor DR (1995) Clay mineral thermometry: a critical perspective. Clay Clay Miner 43:540–553

Essene EJ, Peacor DR (1997) Illite and smectite: metastable, stable, or unstable? Further discussion and a correction. Clay Clay Miner 45:116–122

Esteban M, Taberner C (2003) Secondary porosity development during late burial in carbonate reservoirs as a result of mixing and/or cooling brines. J Geochem Explor 78–79:355–359

Evans AL (1990) Miocene sandstone provenance relations in the Gulf of Suez: insights into Synrift unroofing and uplift history. AAPG Bull 74:1386–1400

Friedmann EI, O'Neil JR (1977) Compilation of stable isotope fractionation factors of geochemical interest. In: Fleischer M (ed) Data of geochemistry, 6 edn. Geol Surv Profes Pap 440-KK. 85 p

Garzanti E, Vezzoli G, Andò S, Castiglioni G (2001) Petrology of Rifted-Margin sand (Red Sea and Gulf of Aden, Yemen). J Geol 109:277–297

Garzanti E, Vezzoli G, Andò S, Dell'Era D (2003) From rifted margins to foreland basins: investigating provenance and sediment dispersal across desert Arabia (Oman, UAE). J Sediment Res 73(4):572–588

Golberg JM, Guiraud M, Maluski H, Seguret M (1988) Caractéres petrologiques êtage du métamorphisme en contexte distensive du bassin sur décrochement de Soria (Crétacé Inferiour, Nord Espagne). C R Acad Sci París, Serie II 307:521–527

Goldstein RH (in press) Fluid inclusion geothermometry in sedimentary systems: from paleoclimate to hydrothermal. In: Harris N (ed) SEPM special publication, Thermal History Analysis of Sedimentary Basins

Goldstein RH, Reynolds TJ (1994) Systematics of fluid inclusions in diagenetic minerals. SEMP Short Course 31. 192 p

Goldstein RH, Rossi C (2002) Recrystallization in quartz overgrowths. J Sediment Res 72(3):432–440

Gómez-Fernández JC, Meléndez N (1994) Estratigrafía de la Cuenca de los Cameros (Cordillera Ibérica Noroccidental, N de España) durante el tránsito Jurásico- Cretácico. Rev Soc Geol Esp 7(1–2):121–139

González-Acebrón L (2009) The Tera Group in the Eastern sector of the Cameros Basin: sedimentary environments, provenance and diagenetic evolution. Dissertation, Universidad Complutense de Madrid, p 424

González-Acebrón L, Arribas J, Mas R (2007) Provenance of fluvial sandstones at the start of late Jurassic-early Cretaceous rifting in the Cameros Basin (N. Spain). Sediment Geol 202:138–157

González-Acebrón L, Arribas J, Mas R (2010) Sand provenance and implications for paleodrainage in a rift basin: the Tera Group. J Iberian Geol 36(1):179–184

Guimerà J, Alonso A, Mas JR (1995) Inversion of an exextensional-ramp basin by a newly formed thrust: the Cameros Basin (N Spain). In: Buchanan, JG, Buchanan PG (eds) Basin inversion. Geol Soc Spec Publ 88, pp 433–453

Guimerà J, Mas JR, Alonso A (2004) Intraplate deformation in the NW Iberian Chain: Mesozoic extension and Tertiary contractional inversion. J Geol Soc London 161:291–303

Guiraud M, Seguret M (1985) A realising solitary overstep model for the late Jurassic- Early Cretaceous (Wealdian) Soria strike-slip basin (Northern Spain). SEMP Spec Publ 37:159–175

Hiemstra EJ, Goldstein RH (2005) The diagenesis and fluid migration history of the Indian Basin Field, Eddy County, New Mexico, In: Lufholm P, Cox D (eds) Unconventional reservoirs, technologies, and strategies, new perspectives for the permian basin. WTGS Publication 05-115, pp 197–206

Hitchon B (1984) Geothermal gradients, hydrodynamics, and hydrocarbon occurrences, Alberta, Canada. AAPG Bull 68(6):713–743

James NP, Choquette PW (1990) Limestones- The meteoric diagenetic environment. In: McIlreath IA, Morrow DW (eds) Diagenesis. Geosci Can, Reprint series, 4, pp 35–73

Kübler B (1967) La cristalinité de l'illite et les zones tout à fait supérieures du métamorphisme. Etages Tectoniques. Coll. Neuchâtel 105–122

Lacazette A (1990) Application of linear elastic fracture mechanics to the quantitative evaluation of fluid-inclusion decrepitation. Geol 18:782–785

Lindhohn RC, Finkehnan RB (1972) Calcite staining: semiquantitative determination of ferrous iron. J Sediment Petrol 42:239–245

Lundergard PD (1992) Sandstone porosity loss. A "big picture" view of the importance of Compactation. J Sediment Petrol 62:250–260

Machel HG, Lonnee J (2002) Hydrothermal dolomite—A product of poor definition and imagination. Sed Geol 152:163–171

Mantilla-Figueroa LC (1999) El metamorfismo hidrotermal de la sierra de Cameros (La Rioja-España): Petrología, geoquímica, geocronología y contexto estructural de los procesos de interacción fluido-roca. Dissertation, Universidad Complutense de Madrid, p 361

Mantilla-Figueroa LC, Casquet C, Mas JR (1998) Los paleofluidos del Grupo Oncala, Cuenca de Cameros (La Rioja, España): Datos de inclusiones fluidas, isótopos de oxígeno y SEM. Geogaceta 24:207–210

Mantilla-Figueroa LC, Casquet C, Galindo C, Mas JR (2002) El metamorfismo hidrotermal Cretácico y Paleógeno de la Cuenca de Cameros (Coordillera Ibérica, España). Zubía. Instituto de Estudios Riojanos 14:143–154

Martín-Closas M, Alonso-Millán A (1998) Estratigrafía y Bioestratigrafía (Charophyta) del Cretácico inferior en el sector occidental de la Cuenca de Cameros (Cordillera Ibérica). Rev Soc Geol Esp 11:253–269

Mas R, Alonso A, Guimerà J (1993) Evolución tectonosedimentaria de una cuenca extensional intraplaca: la cuenca finijurásica-eocretácica de Los Cameros (La Rioja- Soria). Rev Soc Geol Esp 6(3–4):129–144

Mas R, Benito MI, Arribas J, Serrano A, Guimerà J, Alonso A, Alonso-Azcárate J (2002) La Cuenca de Cameros: desde la extensión finijurásica-eocretácica a la inversión terciaria—implicaciones en la exploración de hidrocarburos. Zubía. Instituto de Estudios Riojanos 14:9–64

Mas R, Benito MI, Arribas J, Serrano A, Guimerà J, Alonso A, Alonso-Azcárate J (2003) The Cameros Basin: From late Jurassic- early Cretaceous Extension to Tertiary contractional inversion- implications of hydrocarbon exploration. In: AAPG international conference and exhibition, Barcelona, Spain. Geological Field Trip, vol 11. 52 p

Mas R, García A, Salas R, Meléndez A, Alonso A, Aurell M, Bádenas B, Benito MI, Carenas B, García-Hidalgo JF, Gil J, Segura M (2004) 5.3.3. Segunda fase de rifting: Jurásico Superior-Cretácico Inferior. In: Vera J (ed) Geología de España, Soc Geol Esp—IGME, 503–509

Mata MP, Casas AM, Canals A, Gil A, Pocovi A (2001) Thermal history during Mesozoic extension and Tertiary uplift in the Cameros Basin, northern Spain. Basin Res 13:91–111

Morad S, Ketzer JM, De Ros F (2000) Spatial and temporal distribution of diagenetic alterations in siliciclastic rocks: Implications for mass transfer in sedimentary basins. Sedimentology 47:95–120

Ochoa M, Arribas J, Mas R, Goldstein RH (2007) Destruction of a fluvial reservoir by hydrothermal activity. Sediment Geol 202:158–173

Plata A (1994) Composición isotópica de las precipitaciones y aguas subterráneas de la Península Ibérica: Centro de Estudios y Experimentación de Obras Públicas. Ministerio de Obras Públicas y Transportes, Madrid 140 p

Radke BM, Matthis RL (1980) On the formation and ocurrence of saddle dolomite. J Sediment Petrol 50:1149–1168

Rossi C, Goldstein RH, Ceriani A, Marfil R (2002) Fluid inclusions record thermal and fluid evolution in reservoir sandstones, Khatatba Formation, Western Desert, Egypt: a case for fluid injection. AAPG Bull 86:1773–1799

Rush GB, Reed MH (2005) Scanning electron microscope-cathodoluminiscence analysis of quartz reveals complex growth histories in veins for the Butte porphyry copper deposit, Montana. Geol 30(8):727–730

Rush GB, Reed MH, Dilles JH, Kent AJR, Dypvik H, Goles GG (2006) Intensity of quartz cathodoluminiscence and trace-element content in quartz from the porphyry copper deposit at Butte, Montana. Am Mineral 91:1300–1312

Salas R, Guimerá J, Mas R, Martín-Closas C, Meléndez A, Alonso A (2001) Evolution of the mesozoic central iberian rift system and its cainozoic inversion (Iberian Chain). In: Cavazza W, Roberson AHFR, Ziegler P (eds) Peri-Tethyan Rift- Wrench Basins and Passive Margins. Mém Mus Nat d' Hist Natur 186:145–185

Spötl C, Pitman JK (1998) Saddle (baroque) dolomite in carbonates and sandstones: a reppraisal of a burial-diagenetic concept. In: Morad S (ed) Carbonate cementation in sandstones. IAS Special Publ 26:437–460

Taylor HJR (1974) The applications of oxygen and hydrogen isotope studies to problems of hydrothermal alteration and ore deposition. Econ Geol 69:843–883

Turgarinov AI, Vernadsky VI (1970) Dependance of the decrepitation temperature of minerals on their gas-liquid inclusions and hardness. Akademiya Nauk Doklady 195:112–114

Villalaín JJ, Fernández-González G, Casas AM, Gil-Imaz A (2003) Evidence of a Cretaceous remagnetization in the Cameros Basin (North Spain): implications for basin geometry. Tectonophys 377:101–117

Waples DW (1980) Time and temperature in petroleum formation: application of Lopatin's method to petroleum exploration. AAPG Bull 64:916–926